J Mater Sci (2022) 57:20957–20973

Metals & corrosion

Interface-mediated shear behavior of bonded aluminum substrates

Milad Khajehvand[1,*], Henri Seppänen[2], and Panthea Sepehrband[1]

[1] Department of Mechanical Engineering, Santa Clara University, Santa Clara, CA 95053, USA
[2] Kulicke & Soffa Industries, Inc., Santa Ana, CA 92705, USA

Received: 30 May 2022
Accepted: 3 November 2022
Published online: 16 November 2022

ABSTRACT

Molecular dynamics simulations are utilized to study the shear deformation behavior of aluminum interfaces formed through jump-to-contact (JC) mechanism. In the presence of misorientation between substrates, when shear is applied, (111)-oriented systems exhibit resistance-free sliding, whereas in the (001)- and (110)-oriented systems, dislocation multiplication (DM), which originates from the network of interfacial dislocations, is found to be the controlling mechanism. It is observed that by a decrease in the misorientation angle or an increase in the strain normal to the interface (a consequence of JC), more DM occurs. (110)-oriented systems are found to be the most prone system to DM due to the existence of dislocations with Burgers vector of a $< 100 >$ in their interface. Ultimately, using the profile of average atomic volume along the direction perpendicular to the interface, two characterizing parameters are defined: interface volume expansion (IVE) and interface thickness (IT). IVE describes the excess free atomic volume at the interface relative to that in the bulk, and IT is an estimate of the portion of the system that is considered as the interface region (where defects are concentrated). IVE and IT are shown to have a reverse and direct relationship with the shear strength of the system, respectively, and therefore are introduced as new tools for prediction of shear deformation behavior. Calculation of the IVE and IT parameters enables linking the microscopic characteristics of the interface to shear deformation behavior, which is a controlling phenomenon in various applications. Particularly, the IT parameter is found to be very promising as the direct relationship between IT and shear strength is shown to be independent of the orientation of the interface plane.

Handling Editor: Megumi Kawasaki.

Address correspondence to E-mail: mkhajehvand@scu.edu

https://doi.org/10.1007/s10853-022-07926-x

Introduction

In many joining techniques, especially in ultrasonic bonding [1, 2] and friction welding [3, 4], contact area between two metallic parts is under shear loading and the resultant friction. Bond between the substrates forms locally, and the localized bonded areas grow during the joining process [1, 2, 5, 6]. Jump-to-contact (JC) is proposed as an atomic-scale mechanism for formation of such localized contacts [7]. During the JC phenomenon, atomic layers on the surface of two metallic substrates that are positioned close enough from one another jump toward each other and form a contact. Occurrence of JC is the result of a competition between attractive forces among surface atoms on the opposing substrates and the adhesive forces between atoms on the neighboring layers in the bulk material [7]. The localized contacts that form through JC are particularly important when the bonded areas are under shear loading and experience friction. It is known that, at nanoscale, a transition from a linear to nonlinear dependency of friction force on load takes place if such adhesive contacts exist [8, 9].

Occurrence of JC has been detected through both experimental [10–14] and computational [7, 14–16] studies. In practice, when JC happens, substrates reach each other at an angle and an interface is formed. Interfaces, in general, play an important role in defining material properties and dictating the deformation behavior through various mechanisms. For instance, the intersections of dislocations in a semi-coherent interface or in a small-angle twist grain boundary (GB) can act as sinks for point defects [17, 18]; the dislocation network at an interface can also act as sites for nucleation of partial dislocations [16, 19, 20]. In addition, GBs contribute to inelastic deformation through GB sliding and GB migration [21]. The structure of the GB and whether it is flat or faceted can affect the shear strength of the material [22]. It has also been shown that deformation mechanisms are strongly linked to the existence of free volume in the GB and its distribution [23–25].

The interface that forms thorough JC is similar to a GB. However, due to the gap that exists prior to occurrence of the jump, the JC interface is strained and as a result, the extent and nature of its effect on the material's behavior is different. Unlike GBs that have been extensively studied, the information on the interfaces that form after JC is relatively sparse. It is known that crystallographic orientation plays an important role in how easily and promptly JC occurs [26]. In our earlier works [15, 16], JC between (111)-oriented substrates at multiple angles is studied. It is shown that when the misorientation angle between the substrates (θ) is small, the interface is composed of a dislocation network. While the general pattern and distribution of the interfacial dislocations is a function of θ, their density is found to be a function of both θ and the elastic strain in the system ($\in_{JC}$) that is caused by the initial gap prior to the jump. Moreover, it is seen that primarily due to the existence of $\in_{JC}$, and depending on how low θ is and how high the temperature is, the interfacial dislocations, immediately after contact formation, can multiply and move from the interface region into the bulk. The dislocation multiplication (DM) can happen by nucleation of new dislocations from the interface in low-stacking-fault-energy materials or by cross-slip of the interfacial dislocations in high-stacking-fault-energy materials.

Based on the studies on bicrystals under shear loading [22, 24, 25, 27–29], it is known that GBs have a significant role in controlling plastic deformation in metallic materials through various mechanisms, including dislocation emission from GB [19, 21], GB sliding [21, 30, 31], and GB migration [21, 32]. However, to the best of our knowledge, no attention has been given to understanding the atomic-scale mechanisms of plastic deformation when the JC interface is under shear loading. Specifically, it is important to understand how the dislocations that can multiply right after JC (due to the existence of $\in_{JC}$) evolve upon application of shear.

The objective of the present work is to study the deformation behavior and evolution of dislocations during an application of shear parallel to the interface of two pre-joined aluminum substrates bonded through the JC mechanism. The small-scale (nanoscale) and short duration ($\sim$ fs) of JC [7] makes molecular dynamics (MD) simulations a proper choice for this study. The main parameters in this work are: 1) the crystallographic orientation of substrates ((111), (001), or (110) fcc planes along the thickness), 2) θ, and 3) $\in_{JC}$. Additionally, the characteristics of the profile of average atomic volume along the thickness of the system are linked to the distribution of dislocations and then used to explain the shear deformation behavior.

Computational methods

The simulation procedure is schematically shown in Fig. 1, and Table 1 shows the key simulation parameters and the values used for them in the simulations. To prepare the initial atomic configurations for MD simulations, one aluminum superlattice with face-centered cubic crystal structure is created which contains 48 atomic layers along the z direction of the simulation box. The crystallographic orientation of these atomic planes along the z direction of simulation box is one of the three main parameters in this study. The orientation is either (111), (001), or (110). In all three cases, the crystallographic orientation along the x direction is $[1\bar{1}0]$. Next, this superlattice is divided into two smaller superlattices of the same size (i.e., each with 24 layers along the z direction). To incorporate the second parameter of the study into simulations, i.e., misorientation angle, the two superlattices are rotated about the z axis of simulation box by θ degrees relative to each other. Four misorientation angles of 0°, ∼ 2.45°, ∼ 4.40°, and ∼ 6.00° are chosen for simulations. Only small misorientation angles are used in this work as variation among small angles more significantly influences the network of interfacial dislocations and the distribution and density of interfacial defects following JC [15]. Then, a portion of the system is cut along the x and y directions, so that the system is periodic along those two directions of the simulation box. The resulted structure in all cases is then replicated along the x and y directions so that at least 300,000 atoms exist in the simulations.

Afterward, the two substrates are placed far away from one another to ensure that they do not apply force on each other. System's energy is minimized using the conjugate gradient method and the system is thermalized at 300 k in an NPT (i.e., fixed number of atoms, pressure, and temperature) ensemble. Next, the substrates are brought closer to each other and positioned at various interfacial distances from one another, and simulation is run modeling an NPT ensemble. If the initial distance between substrates' free surfaces is less than or equal to the critical distance for JC, JC occurs. The critical distance for JC for different cases is calculated using a similar approach to our earlier studies [15, 16]. The values of critical distance for JC for (111), (001), and (110) cases are found to be 2.4, 3.0, and 4.0 times the distance between adjacent (111), (002), and (220) planes in a perfect unstrained aluminum crystal. After occurrence of JC, a tensile elastic strain perpendicular to the interface exists in the system which its value is a function of the initial interfacial distance. The strain value, i.e., $\in_{JC}$, which is the third parameter in this study, can be calculated from the following equation:

$$\in_{JC} = \frac{1}{2} \times \frac{h_{final} - h_{initial}}{23 \times z_{[hkl]}} \quad (1)$$

In this equation, $z_{[hkl]}$ is the distance between adjacent planes along the $[hkl]$ fcc direction in a perfect unstrained crystal ($z_{[111]} = 2.34\text{Å}$, $z_{[001]} = 2.03\text{Å}$,

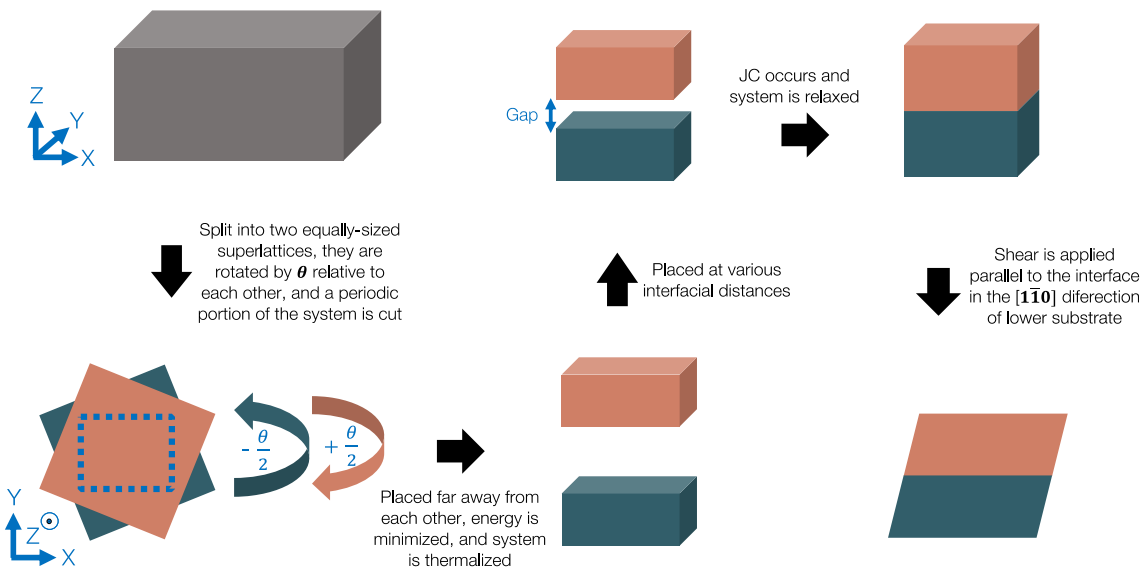

Figure 1 Schematic of the simulation procedure.

Table 1 Simulation parameters and their values

Parameter	Values
Crystallographic orientation of the interface plane	(111), (001), (110)
Misorientation of substrates relative to each other, θ	0°, ~ 2.45°, ~ 4.40°, ~ 6.00°
Strain normal to the interface due to jump-to-contact, $\in_{JC}$	1.5%, 2.0%, 2.5%

and $z_{[110]} = 1.43$Å), h_{final} is the interfacial distance after occurrence of JC and can be approximated to be equal to $z_{[hkl]}$, and h_{initial} is the initial interfacial distance which can be set to be a multiple of $z_{[hkl]}$. Although JC occurs rapidly (on the order of fs) [7], this step of simulation is run for 200 ps to ensure that the system is relaxed before application of shear.

To observe the shear deformation behavior of different systems, after JC is occurred and the system is relaxed, shear is applied parallel to the interface of the joined substrates in the $[1\bar{1}0]$ direction of the lower substrates. This direction is $-\theta/2$ off from the positive x axis of simulation box. $[1\bar{1}0]$ direction is chosen because it is the direction of the Burgers vector of perfect dislocations in the crystal and it is contained in the plane of interface for all three orientations studied. For applying shear, simulation box is slanted in a sinusoidal fashion, i.e., shear strain is not a linear function of simulation time. A quarter of a single vibration cycle is used instead of a constant shear strain rate so the outcome of this work can be extended for studying the application of multiple cycles of vibration to the interface. The maximum shear strain (in the final state of simulations) is set to be 0.25. This level of strain is found to be enough for initiating plastic deformation in all cases. The maximum shear strain divided by simulation time is set to be 0.001 ps^{-1}, which is comparable with the values used in similar MD studies [24, 33].

MD simulations are performed using the Large-scale Atomic/Molecular Massively Parallel Simulator (LAMMPS) simulation package [34] and embedded atom method interatomic potential for aluminum [35]. Timestep of 0.002 ps is used for time integration of equations of motion. Nosé-Hoover thermostat and barostat [36–38] are used for keeping the temperature and pressure (along the periodic directions) constant. Periodic boundary conditions are used along the x and y directions. The uppermost layer of top substrate and the lowermost layer of bottom substrate are kept fixed during simulations. During thermalization, JC occurrence and the relaxation after that, the other 23 layers per substrate are treated as NPT layers. However, when shear is applied, the 2 layers adjacent to the fixed layer are NVT layers, while the other 21 layers are NVE layers. The reason for doing this is that during application of shear, thermostating in the system is done somewhere far away from the interface, so that phenomena happening in the interface region are not directly affected. The identification of the exact character of interfacial dislocations in this work is done using the dislocation analysis modifier [39] of OVITO [40]. An alternative and possibly more informative way for dislocation characterization is the disregistry analysis (similar to what is done in [41]), but that is beyond the scope of this work.

To connect the general characteristics of the network of interfacial dislocations, formed after JC, to the shear deformation behavior, two important characteristics of the interface, interface volume expansion and interface thickness, are defined and used in this work. The former is an indication of the difference in the average atomic volume at the interface and inside the bulk, and the latter expresses the thickness of the space near interface with higher average atomic volume than the bulk. To quantify these two characteristics, initially, Voronoi analysis is used to calculate the volume that is occupied by each atom in the system. Then, the profile of average atomic volume as a function of normalized z position, shown in Fig. 2 for one simulation as an example, is generated. Normalized z position for each atom is calculated by subtracting the minimum z position of all atoms from the z position of the atom and dividing the result by the thickness of the system, i.e., l_z. The bulge seen on the atomic volume profile in Fig. 2 is due to the presence of crystallographic defects, which are generated as a result of misorientation between substrates, at the interface. Therefore, it is reasonable to use the characteristics of this bulge, i.e., its height and width, to define the interface properties. By fitting a Gaussian distribution formula to the data and obtaining the constants for it, the interface

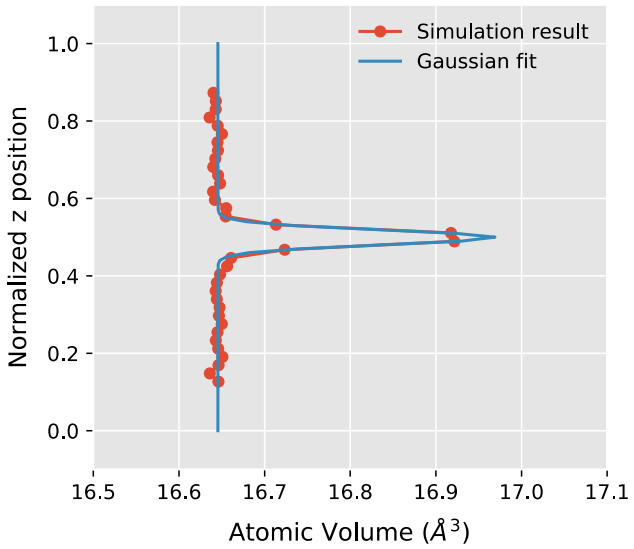

Figure 2 The profile of average atomic volume along the thickness of the system and the fitted Gaussian distribution for a simulation with (111)-oriented substrates, 2.45° θ, and 1.5% $\in_{JC}$, right before application of shear. Interface is where the normalized z position is equal to 0.5.

volume expansion (IVE) and interface thickness (IT) are defined and calculated as follows:

$$\mathrm{IVE}(\%) = \frac{V_{\mathrm{interface}} - V_{\mathrm{bulk}}}{V_{\mathrm{bulk}}} \times 100 \tag{2}$$

$$\mathrm{IT}(\%) = \text{full width at tenth of maximum}\left(\text{peak value}\right) \times 100 = 2\sqrt{2\ln 10} \times \text{standard deviation} \times 100 \tag{3}$$

where $V_{\mathrm{interface}}$ and V_{bulk} are the average atomic volume at the interface (peak value) and inside the bulk (base value), respectively.

Results and discussion

Shear deformation behavior

To understand the shear behavior of the system, the profile of shear strain during deformation is analyzed. For this purpose, shear is applied parallel to the interface and the localized level of shear strain throughout the thickness of the structure is analyzed through generating "normalized z position vs. shear strain" scatter plots. Shear strain is calculated for any atom by dividing its displacement in the direction of applying shear by the thickness of the system using the equation $\gamma = (\Delta x \times \cos(-\theta/2) + \Delta y \times \sin(-\theta/2))/l_z$, where Δx and Δy are the displacement of the atom along the x and y directions, respectively. The next three subsections make use of the "normalized z position vs. γ" scatter plots and discuss the effect of orientation, misorientation, and $\in_{JC}$ on the shear deformation behavior of system, respectively.

Shear behavior in the absence of misorientation

The shear deformation behavior of the system, in the absence of misorientation, is analyzed in this section. Fig. 3 shows the "normalized z position vs. γ" plots for three simulations with no θ, same level of $\in_{JC}$, but different crystallographic orientations. Atoms are colored differently based on whether they are located in the lower or upper substrate and whether they are fixed (dark blue or maroon), NVT (orange or gray), NVE/bulk (green or yellow), or NVE/surface (purple or light blue) atoms. On the "normalized z position vs. γ" plots, the slope of an imaginary line that connects atomic layers together is an indication of the total level of strain in the system along the direction of shear. Initially, at low level of strains, all systems behave similarly, where γ is a linear function of normalized z position showing that deformation is distributed throughout the thickness uniformly (Fig. 3(a), (e), and (i)). However, at higher level of deformations, the linear relationship between γ and normalized z position no longer exists, and the plots look different for the three cases. The deviation from linear behavior is an indication of occurrence of localized deformation that can be linked to plastic deformation through dislocation activities. It should be noted that based on Fig. 3(b), (f), and (j), plastic deformation is started at different values of γ in the three systems, which is also in agreement with our observation from the "shear stress vs. shear strain" plots (not presented here). Systems with different orientations are dissimilar in terms of their plastic deformation behavior. As seen in Fig. 3(b)–(d), for (111), scattering is mostly along the shear strain axis; for (110), scattering is mostly along the normalized z position axis (Fig. 3(j)-(l)); and for (001), the behavior is something between the behavior of the other two orientations (Fig. 3(f)-(h)). Scattering along the shear strain axis suggests an occurrence of slip parallel to the interface, whereas scattering along the normalized z position axis or any scattering that is not purely along the shear strain axis is an indication of slip on a plane that is not exactly parallel to the plane of the interface.

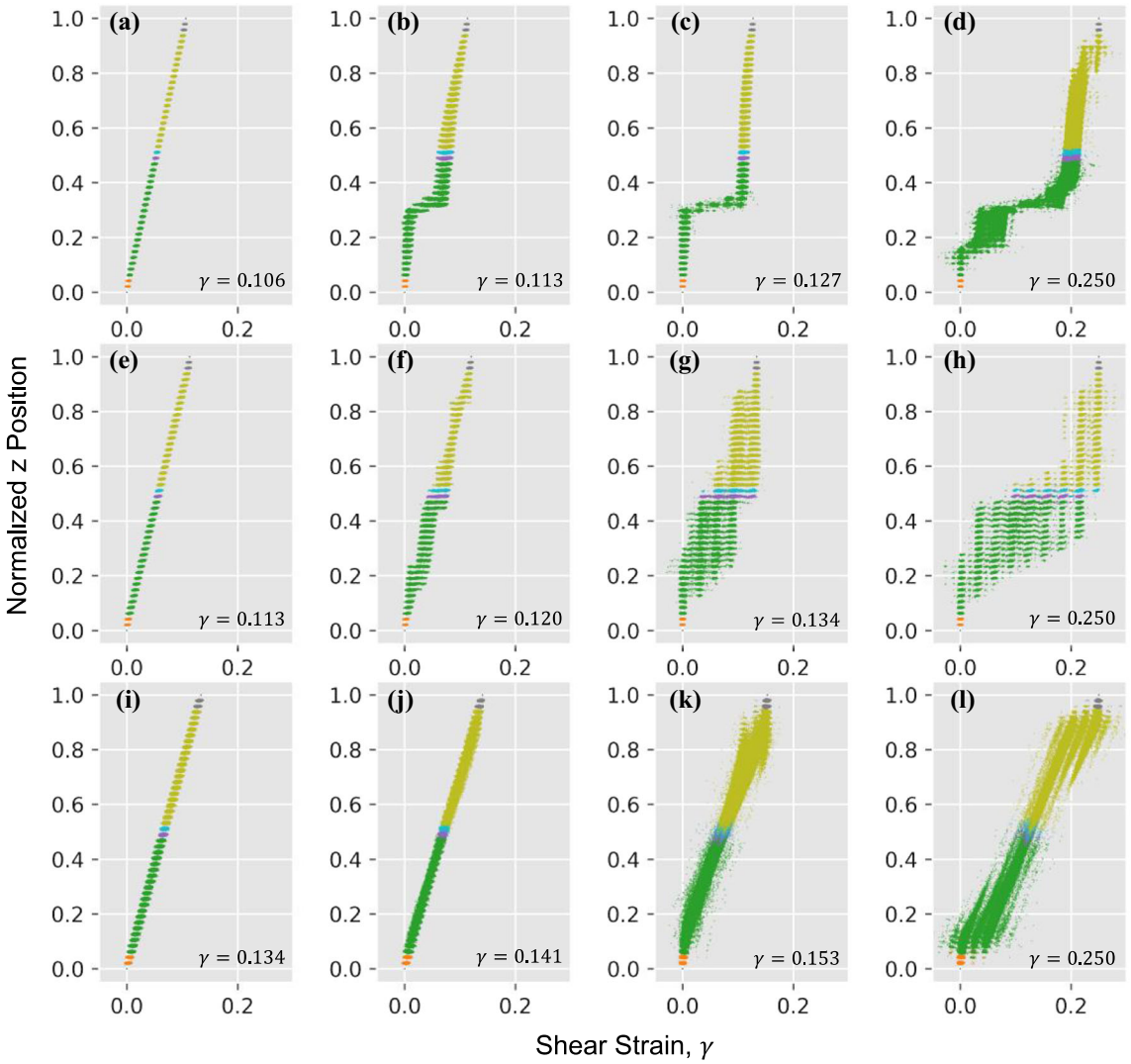

Figure 3 "normalized z position vs. shear strain" scatter plots, showing the change in the profile of shear strain (γ) during the simulation as a function of shear strain (γ), for 0° misorientation, 1.5% $\in_{JC}$, and three interface planes: **a**–**d**: (111), **e**–**h**: (001), and **i**–**l**: (110). Atoms are colored differently based on whether they are originally in the lower or upper substrate and whether they are fixed (dark blue or maroon), NVT (orange or gray), NVE/bulk (green or yellow), or NVE/surface (purple or light blue) atoms.

The difference in the behavior of the three systems can be explained by considering the orientation of the four (111) primary slip planes with respect to the plane of interface. For (111) orientation, one slip plane coincides with the plane of interface and the other three planes are located at 70.53° angle from the interface plane. Since shear is applied parallel to the interface, slip starts on a (111) plane parallel to the interface (in this case, somewhere inside the bulk of the lower substrate as can be seen on Fig. 3(b)). This is also confirmed by visualization of the simulation and observing the partial dislocations being generated and gliding on that plane. As shown in Fig. 3(b) and (c), the slip parallel to the interface causes the layers above the slip plane to go to right and the layers below that plane to go to the left. Later, in Fig. 3(d), dislocations also glide on the other three slip planes that are not exactly parallel to the interface, and this causes scattering along the y-axis, which in turn makes the atomic layers becoming less discernible from one another. When orientation is (001), three slip planes are at a 54.74° angle from the plane of interface, and the other one has a 125.26° angle with it. A vector at a 54.74° angle from the interface has components both contained at the interface and perpendicular to it. Therefore, for this

system, scattering along both x and y axes is observed. Lastly, for the (110) case, two of the primary slip planes are perpendicular to the plane of interface and the other two are at an angle of 35.26° from it. As observed in the visualization of simulation, for this system, slip is initiated mostly on the planes perpendicular to the interface. This is interesting because although shear is applied parallel to the interface (which makes slip on the 35.26° planes more favorable), slip is initiated on the planes perpendicular to the interface, which shows the significant effect of $\in_{JC}$ on this system. Consequently, after initiation of plastic deformation (see Fig. 3(j)), atoms are only scattered along the y-axis. As a result of this spread, atomic layers become less detectable from each other. Later in Fig. 3(k) and (l), slip also happens on other slip planes and this results in the displacement of atoms having a component along the direction parallel to the interface as well.

Shear behavior in the presence of misorientation

As discussed in the previous subsection and shown in Fig. 3, when θ is 0°, plastic deformation does not necessarily start at the interface. This is because the interface does not possess a higher density of defects, compared to the bulk. Therefore, the interface is not significantly weaker than the other regions of the system. But the situation is quite different when θ is not equal to 0°. To study the effect of θ on the shear deformation behavior, nine cases with different orientations and different nonzero θ s, but with the same level of $\in_{JC}$, are simulated. Fig. 4 shows the "normalized z position vs. γ" plots corresponding to the final state (i.e., at the end of shear application) of those simulations. According to Fig. 4(a)-(c), for the (111) orientation, irrespective of θ, the part of the system above the interface moves on top of the lower part almost rigidly, i.e., atomic planes in a particular substrate do not move relative to each other. Also, no scattering of the atomic layers is observed perpendicular to the interface, and they all are detectable from each other at the end of the simulation. These observations show that for this case, shear is compensated through sliding of the two substrates. Also, comparing Fig. 3(d) and Fig. 4(a), it is seen that the presence of misorientation significantly affects the shear deformation behavior of the (111) system. When misorientation exists between the substrates, the interface is the weak point of the system and deformation is mainly concentrated at the interface. In other words, plastic deformation happens by sliding at the interface, as opposed to the occurrence of slip inside the bulk for the case with 0° misorientation angle. For (001) orientation, the plastic deformation is also concentrated near the interface (Fig. 4(d)-(f)). However, for this system, a small level of scattering of atoms is observed along both x and y axes in a thin region near the interface. The fact that plastic deformation is happening along directions not exactly parallel to the interface, in addition to our prior knowledge on existence of a network of dislocations at the interface of two misoriented substrates [15, 16], suggests that plastic deformation for this case occurs through dislocation activity which is initiated through dislocation multiplication (DM) originated from the network of interfacial dislocations. Dislocations nucleate at the interface and glide toward the bulk on planes intersecting with the plane of interface. The (110) case is similar to the (001) case in terms of the mechanism for plastic deformation, but as the region near the interface that is affected by DM is thicker compared to (001), it can be concluded that (110) is more prone to DM. Additionally, in Fig. 4(d)-(i), it is seen that the thickness of the region wherein the atomic arrangement is highly affected by deformation decreases as θ increases. So, for the (001) and (110) orientations, deformation gets more concentrated at the interface by increase in θ, i.e., the degree of DM decreases by increase in θ.

To accurately identify the occurrence of DM during shear, the evolution of total dislocation density throughout the simulation is analyzed. DM happens if an increase in the value of the total dislocation density is detected. Fig. 5 shows the evolution of total dislocation density as a function of γ for some of the cases studied in Fig. 4. It is seen that when shear is applied, DM does not occur for (111), slightly occurs for (001), and significantly occurs for (110). This observation confirms the findings from the "normalized z position vs. γ" plots. Moreover, for the (001) and (110) cases that DM occurs, it is seen that as θ increases, the rate of increase in the total dislocation density during shear decreases, i.e., the amount of DM is found to have a reverse relationship with θ. However, the initial value of the total dislocation density right after JC (i.e., at $\gamma = 0$), has a direct relationship with θ, as also reported in our previous works [15, 16].

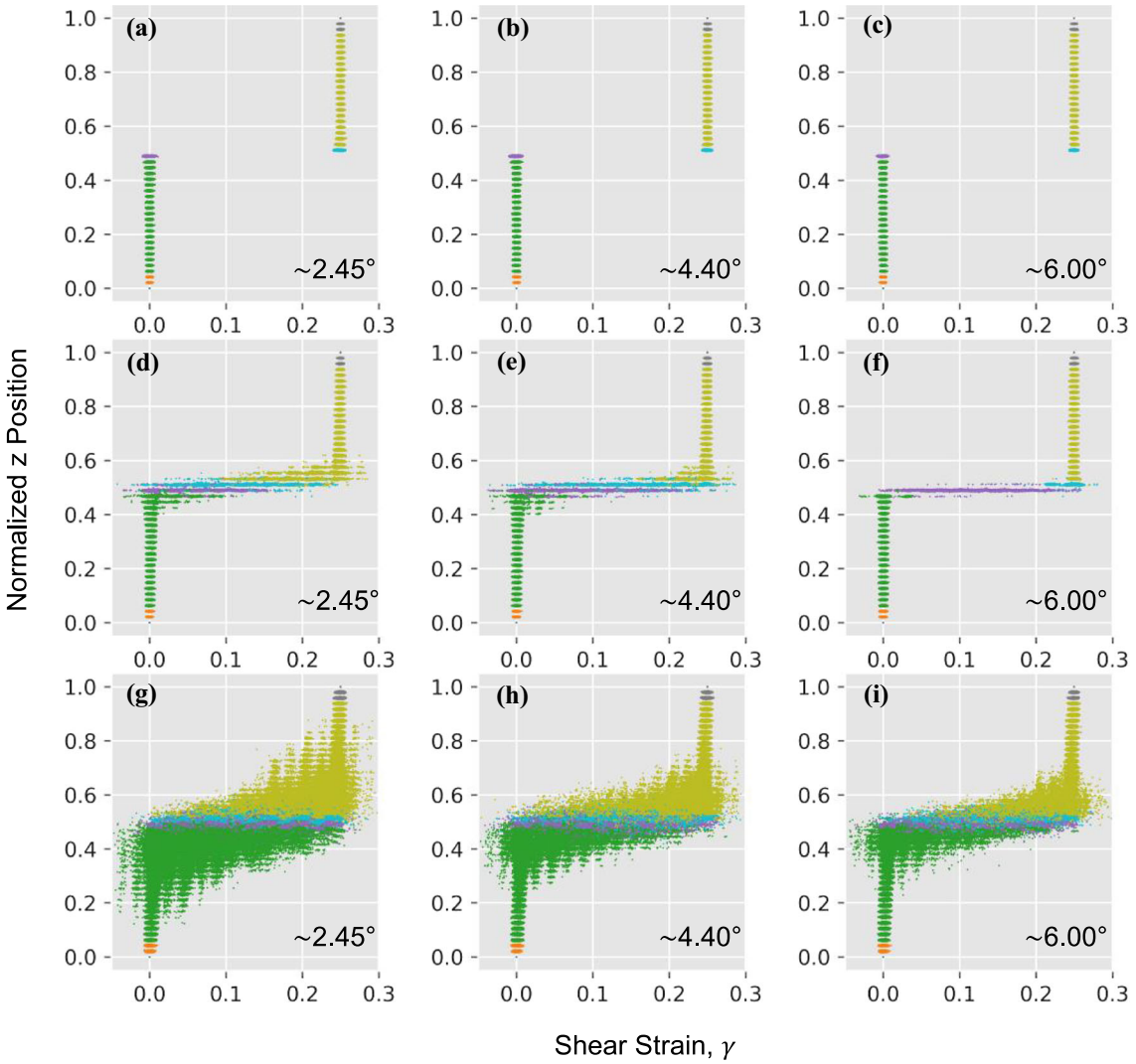

Figure 4 "normalized z position vs. shear strain" scatter plots, showing the effect of orientation and misorientation (θ) on the profile of shear strain. The interface planes are: **a**–**c**: (111), **d**–**f**: (001), and **g**–**i**: (110). The level of strain due to JC is equal to 1.5% in all cases. Atoms are colored differently based on whether they are originally in the lower or upper substrate and whether they are fixed (dark blue or maroon), NVT (orange or gray), NVE/bulk (green or yellow), or NVE/surface (purple or light blue) atoms.

Effect of initial gap size on shear behavior

The gap size can be translated to an equivalent level of tensile elastic strain applied perpendicular to the interface, i.e., $\in_{JC}$. In Fig. 6, the final states (i.e., at the end of shear application) of nine simulations with different orientations and levels of $\in_{JC}$, but similar θ, are shown. For all cases, for a given crystallographic orientation, similar behavior is observed irrespective of the level of strain. Therefore, it can be implied that the mechanism of deformation is not a function of $\in_{JC}$, at least for the range of the strain studied. Additionally, for (110) orientation, in which the interface significantly resists shear, the higher the $\in_{JC}$ is, the more DM happens. Although the same trend is not very clear for the (001) orientation, the same behavior is expected, and the lack of clarity is mostly due to the fact that the amount DM for this orientation is very limited. To better describe the situation, the evolution of the total dislocation density as a function of γ is studied and the results are shown in Fig. 7. It is seen that DM indeed happens in (001), but as expected, to a lower extent compared to (110). It is observed that for the cases that DM happens, and particularly for the (110) orientation, the amount of increase in the total dislocation density throughout the simulation rises by the increase in $\in_{JC}$. Therefore, higher $\in_{JC}$ results in higher amount of DM

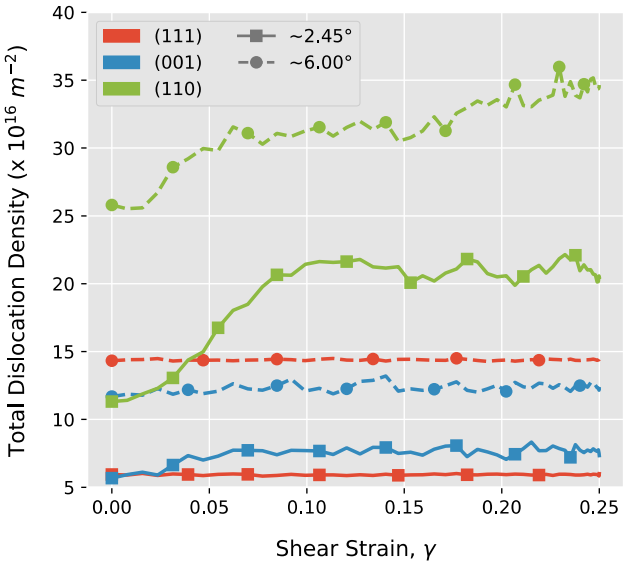

Figure 5 Evolution of total dislocation density as a function of shear strain, showing the effect of misorientation. For all simulations, the level of strain due to JC ($\in_{JC}$) is 1.5%.

occurrence. It is also seen that the initial density of dislocations right after JC (i.e., $\gamma = 0$) is a function of $\in_{JC}$, as also reported previously [15, 16]. Combining the analysis here and the one made in the previous subsection, it may be concluded that the increase in $\in_{JC}$ and decrease in θ have the same effect on the amount of DM, but the effect of θ is more significant.

Shear strength

As discussed earlier, for the (111) case, deformation happens very easily. The almost freely slide of the two substrates on top of each other may be an indication of a very low shear strength for this case. On the other hand, the (001) and especially (110) cases seem to be more resistive to shear deformation. To track resistance to shear for the cases that are studied, the "shear stress vs. shear strain" graphs are made. Shear stress is calculated using the equation $\tau = \left(F_x \times \cos(-\theta/2) + F_y \times \sin(-\theta/2)\right)/A$, where F_x and F_y are the force sensed by the atoms on the fixed layer of the lower substrate along x and y directions of simulation box, respectively. And, A is the area of xy plane in the simulation cell. The value of stress right before the first drop in stress values on the above-mentioned graphs, i.e., shear strength, can be considered as a measure for the resistance to shear of the system. Shear strength values of 2.03 GPa, 2.19 GPa, and 3.20 GPa are calculated for the (111)-, (001)-, and (110)-oriented cases with no misorientation and 1.5% $\in_{JC}$, respectively. All calculated shear strengths are sufficiently lower than the ideal shear strength of aluminum (i.e., theoretical shear strength of aluminum without imperfections $\sim$ 3.67–3.83 GPa [42]). Interestingly, when compared to a single crystal (under the same loading condition), (111) case with 0° misorientation angle and 1.5% $\in_{JC}$ has a lower shear strength (2.03 GPa compared to $\sim$ 3.15 GPa [33]). This comparison implies that even in the absence of misorientation (and a detectable interface), solely due to the $\in_{JC}$ shear strength is reduced.

Additionally, the shear strength values for the cases with misorientation are presented in Fig. 8. The calculated values are within the same order of magnitude as the shear strength values for the twist GBs with the same orientations [22]. The results confirm that the (110)-oriented cases have the highest shear strength, and (111) ones have a shear strength very close to zero, which is an indication of no resistance to shear at the interface. The shear strength values generally follow the (111) < (001) < (110) order. This observation can be explained in a few different ways. First and foremost, the interplanar spacing of adjacent planes along the [111], [001], and [110] direction in a perfect aluminum crystal at 300 K, is equal to 2.34 Å, 2.03 Å, and 1.43 Å, respectively. Larger spacing between adjacent planes makes it is easier for them to slide on one another. Secondly, the energy of aluminum twist GBs follows the same order of (111) < (001) < (110) [43, 44]. Since generally a linear relationship exists between GB energy and GB free volume [22, 45, 46], similar to the previous reasoning, an interface with higher energy is expected to have lower shear strength. Lastly, the trend is in agreement with what reported for aluminum twist GBs. Bomarito et al. [22] calculated the shear strength of 343 aluminum twist GBs with many different orientations and showed that (111) and (001) GBs generally have the lowest shear strengths. They found out that (111) and (001) GBs, unlike most GBs, have a very flat structure. A flat interface is potentially less resistant to shear because the two sides of the interface can slide more easily relative to each other.

It is seen in Fig. 8 that as θ increases, shear strength reduces. On the other hand, the initial gap size seems to not have a significant effect on shear strength, at least for the range of values used in this work. Combination of the above findings shows that as

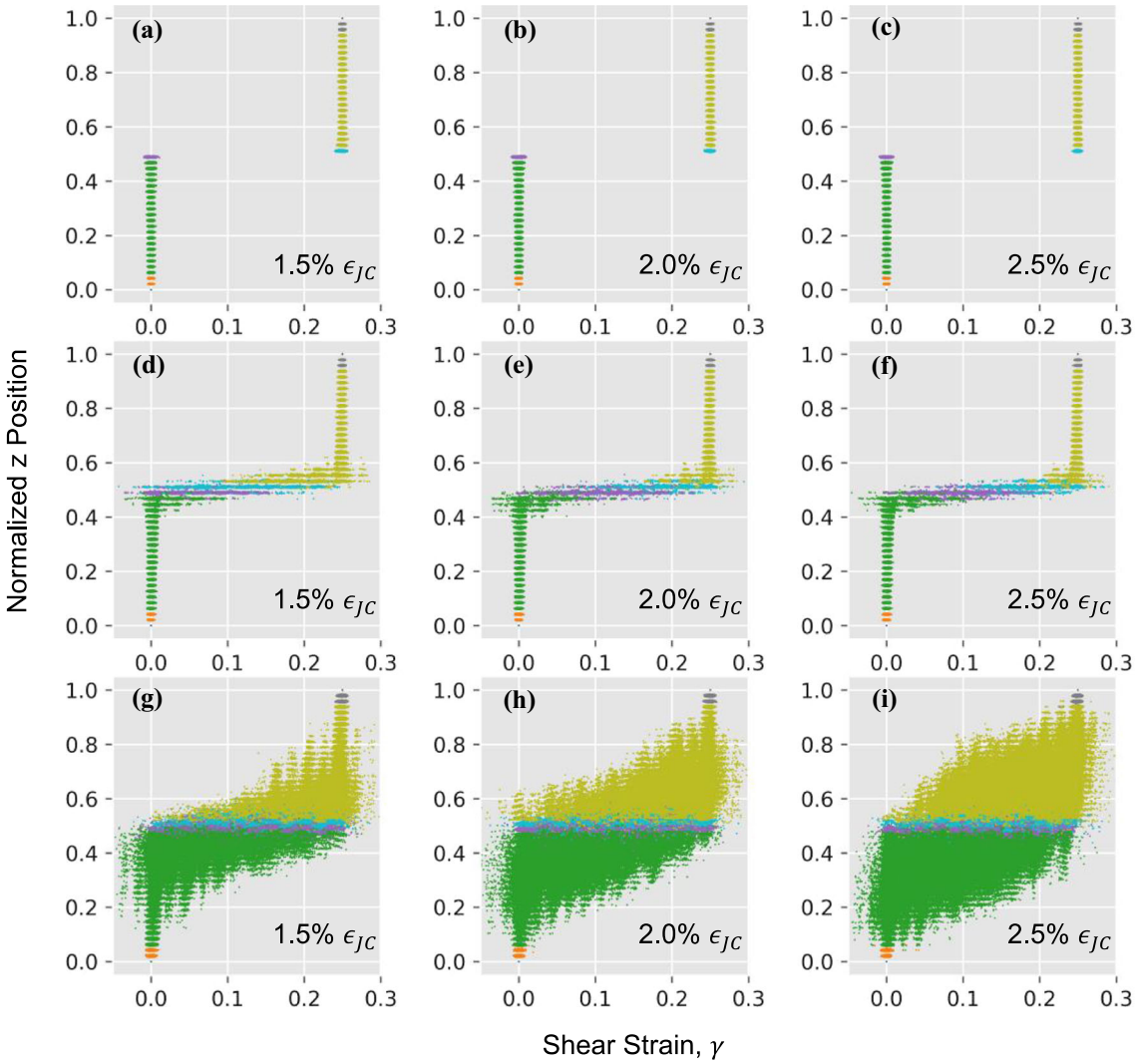

Figure 6 "normalized z position vs. shear strain" scatter plots, showing the effect of orientation and $\in_{JC}$ on the profile of shear strain. The interface planes are: **a**–**c**: (111), **d**–**f**: (001), and **g**–**i**: (110). Misorientation is ~ 2.45° in all cases. Atoms are colored differently based on whether they are originally in the lower or upper substrate and whether they are fixed (dark blue or maroon), NVT (orange or gray), NVE/bulk (green or yellow), or NVE/surface (purple or light blue) atoms.

proposed, the resistance to shear is a strong function of orientation and to a lesser extent misorientation.

Mechanism of DM

In the presence of a small θ, the interface of two substrates after occurrence of JC contains a network of dislocations. To understand the mechanism of DM and to further analyze the shear deformation behavior, the evolution of the network of interfacial dislocations throughout the simulation is analyzed. The network of interfacial dislocations after JC and right before application of shear, is shown in Fig. 9, for three simulations with different orientations, but similar θ (about 2.45°) and same $\in_{JC}$ (1.5%). The images in the first, second, and third rows show the top, side, and perspective views of the same dislocation network. Dislocations are colored based on their type, where Shockley partial dislocations with Burgers vector of a/6 < 211 > are shown in green, perfect dislocations with Burgers vector of a/2 < 110 > are shown in blue, and dislocations with Burgers vector of a < 100 > are shown in red color. The dislocation networks observed are consistent with the literature on twist GBs [32, 47–49]. As seen in Fig. 9(a) and (g), for (111) orientation, the interface consists of a triangular network of Shockley partial dislocations. Fig. 10(a) shows the same dislocations

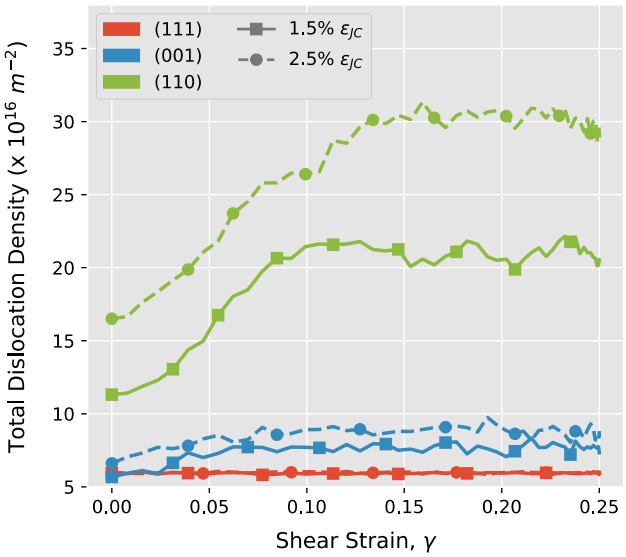

Figure 7 Evolution of total dislocation density as a function of shear strain, showing the effect of $\in_{JC}$. For all simulations, misorientation is about 2.45°.

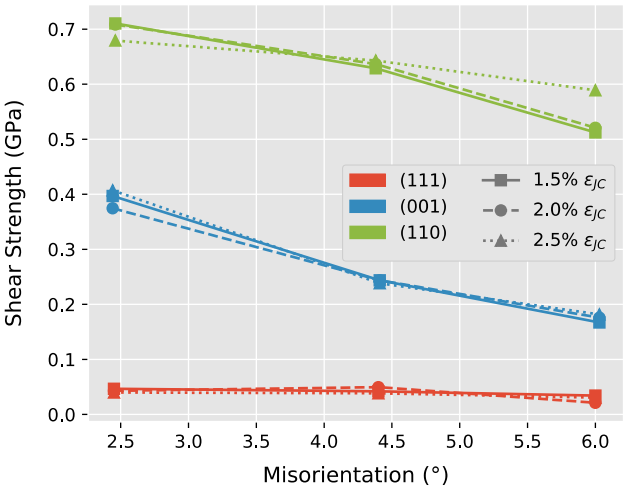

Figure 8 Values of shear strength as a function of misorientation for the cases studied.

where they are colored based on Burgers vector this time. It is seen that the Shockley partial dislocations are three crossing sets of dislocations with Burgers vectors of $\frac{a}{6}[\bar{2}1\bar{1}]$, $\frac{a}{6}[\bar{1}12]$, and $\frac{a}{6}[1\bar{2}1]$. Also, in some locations near the dislocation junctions, Shockley dislocations are recombined, and perfect dislocations are formed. As an example, the Burgers vector of a perfect dislocation is annotated in the figure as $\frac{a}{2}[\bar{1}0\bar{1}]$ ($\frac{a}{6}[\bar{2}1\bar{1}]+\frac{a}{6}[\bar{1}12]\rightarrow\frac{a}{2}[\bar{1}0\bar{1}]$). In addition, to identify the exact character of interfacial dislocations and whether they are edge or screw dislocations, Burgers vectors of dislocations are shown by yellow arrows in Fig. 10(b); Fig. 10(c) is a zoomed-in version of Fig. 10(b). It is seen that all interfacial dislocations are screw dislocations as their Burgers vector is parallel to the dislocation line direction. In the case of (001) and (110) orientations, a square network of perfect dislocations, and a rectangular network of perfect dislocations and dislocations of the type a < 100 > are observed, respectively (see Fig. 9(b), (c), (h) and (i)). A similar analysis to what is done for (111) interface is performed for (001) and (110) interfaces, and it is found out that the interfacial dislocations in those cases are also all screw dislocations.

As seen in Fig. 9(d), the dislocation network for the (111)-oriented system is found to be concentrated at the interface, leading to a thin and sharp interface. On the other hand, it is interesting to note the dislocation dissociation that happens for the (001) and (110) orientations. In addition, for these two cases, as shown in Fig. 9(e) and (f), dislocations are distributed through a thicker width across the interface compared to (111) orientation. These observations suggest that under the same level of $\in_{JC}$, the (001), and especially (110) cases are more prone to DM, compared to the (111) case. Therefore, when shear is applied to these systems, there is a higher chance for it to be compensated through dislocation activities.

DM starts by dislocations dissociating at the interface. Then, the dissociated dislocations (or the result of the interaction between them) glide on the slip planes intersecting the interface. For the (110) case (see Fig. 9(c)), as a result of $\in_{JC}$, which is perpendicular to the interface, some perfect dislocations, and dislocations of the type a < 100 > are already dissociated, even before application of shear. Therefore, when shear is applied, plastic deformation heavily occurs at the areas close to the interface leading to the high level of displacement of atoms in the regions near the interface, as seen in Fig. 4 and Fig. 5. The high propensity to DM in (110)-oriented systems is due to the existence of dislocations of the type a < 100 >, shown by red in Fig. 9(c), which can dissociate into two perfect dislocations, e.g., $a[0\bar{1}0]\rightarrow\frac{a}{2}[1\bar{1}0]+\frac{a}{2}[\bar{1}10]$. These perfect dislocations can further dissociate into two Shockley dislocations or react to other Shockley dislocations.

For the (001) orientation, the dislocation network mainly consists of perfect dislocations. They can split

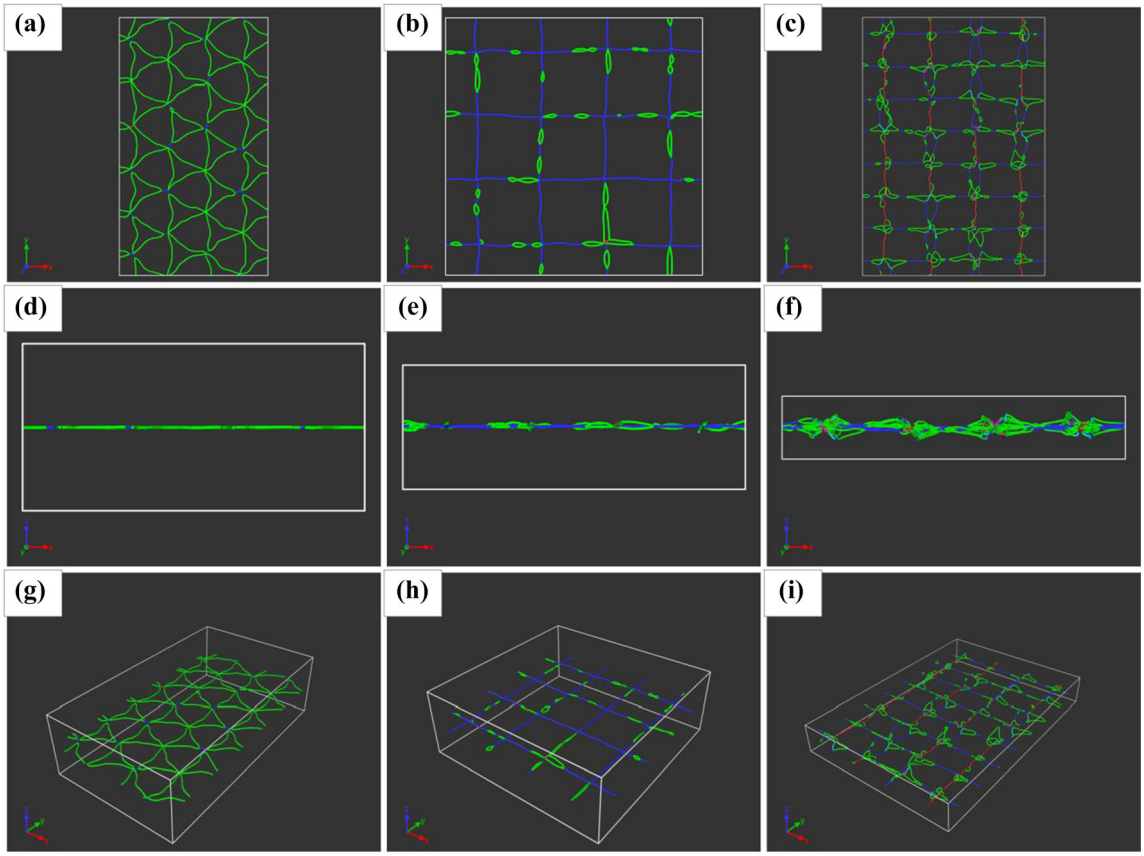

Figure 9 Network of interfacial dislocations right after JC, but before applying shear, for three simulations with different orientations. The interface plane in the simulation of (**a**,**d**, **g**) is (111), for (**b**,**e**, **h**) is (001), and for (**c**,**f**, **i**) is (110). θ is about 2.45° and $\in_{JC}$ is 1.5% for all three simulations. (**a**–**c**) show the top-view images, (**d**–**f**) show the side-view images, and (**g**–**i**) show the perspective-view images. Shockley, perfect, and stair-rod dislocations are shown in green, blue, and pink; any other dislocation is shown in red.

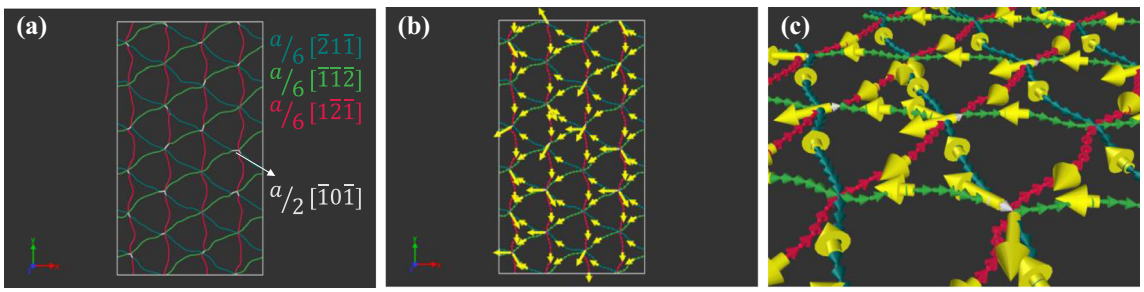

Figure 10 Network of interfacial dislocations right after JC, but before applying shear, for the (111)-oriented system. **a**: the dislocations are colored based on Burgers vectors; **b**: the Burgers vectors for all dislocations are shown by yellow arrows. **c**: a zoomed-in version of **b** showing the direction of dislocation lines and Burgers vectors.

into Shockley dislocations making the occurrence of DM possible, but the extent of DM is not as much as that in the (110)-oriented system. Lastly, in the case of (111) orientation, Shockley dislocations already exist, but they are pinned by the dislocation nodes. DM can occur for this case only if new dislocations nucleate

from the interface, or if cross-slip of interfacial dislocations happens, both of which require higher levels of $\in_{JC}$ [16] that is not present in the cases studied.

Dislocation networks at the final state of deformation ($\gamma = 0.25$) are shown in Fig. 11. It is seen that while dislocation network for (111) remains sharp and clean (Fig. 11(a) and (g)), for the (110) case, the regular rectangular shape of the dislocation network is nearly destroyed (Fig. 11(c) and (i)) and dislocations are gone out of the plane of interface (Fig. 11(f)). As previously seen in other analyses, behavior of (001) is between (111) and (110): the dislocation network is not completely maintained (Fig. 11(b) and (h)) and some level of dislocation movement out of the interface is observed (Fig. 11(e)). These results confirm the previous statements that upon application of shear, DM is much more pronounced in the (110) case, compared to the other cases. While DM is also observed in (001) to some extent, for the (111) case, no DM can be seen even after shear.

Characterizing the interface

It is seen that depending on the nature of the interface, shear deformation may be compensated through either resistance-free sliding of the two substrates relative to each other, or DM accompanied by dislocation glide. Considering this significant role of the interface in dictating deformation mode, the relationship between a more general set of interface characteristics (as opposed to specific simulation parameters) and the behavior of the system during shear loading, especially in terms of shear strength is investigated. For this purpose, the interface is characterized using the two parameters of IVE and IT (see computational methods section for mathematical definition). IVE represents the average volume

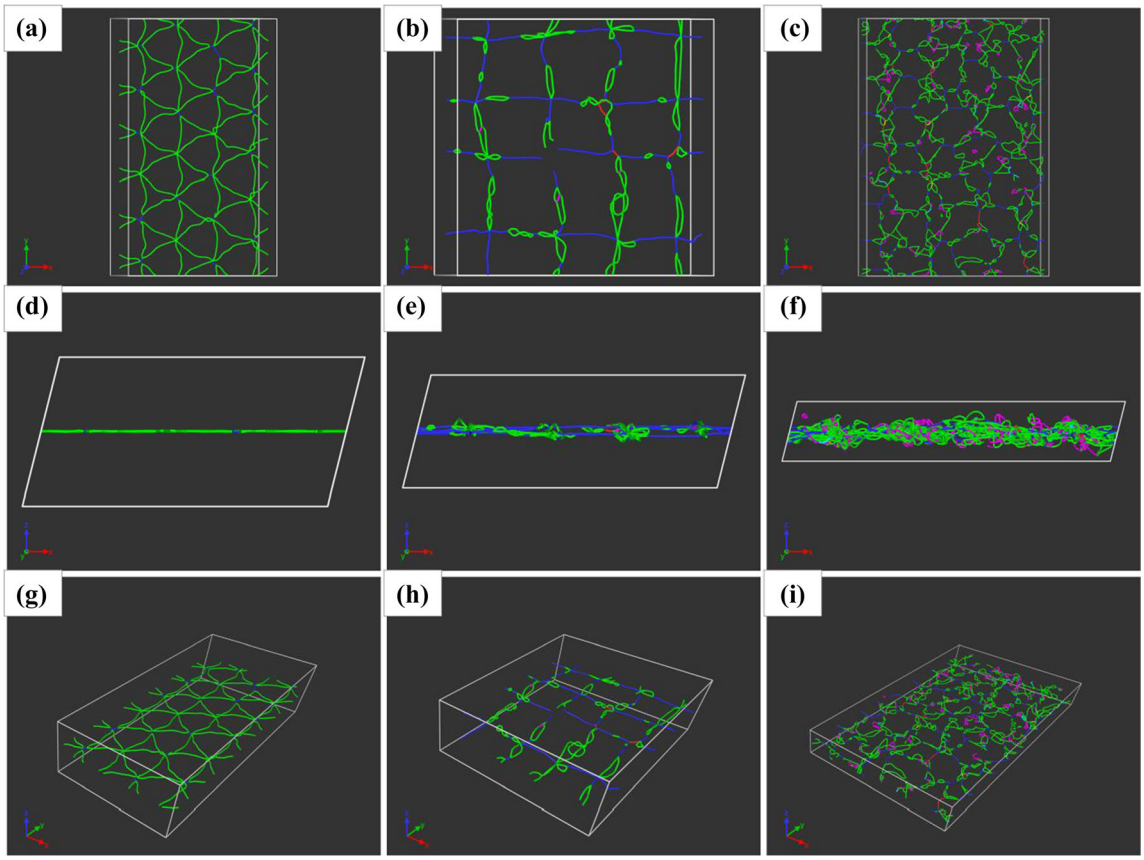

Figure 11 Network of interfacial dislocations at the end of application of shear ($\gamma = 0.25$), for the same three simulations of Fig. 9. The interface plane in the simulation of (**a**,**d**, **g**) is (111), for (**b**,**e**, **h**) is (001), and for (**c**,**f**, **i**) is (110). θ is about 2.45° and $\in_{JC}$ is 1.5% for all three simulations. (**a**–**c**) show the top-view images, (**d**–**f**) show the side-view images, and (**g**–**i**) show the perspective-view images. Shockley, perfect, and stair-rod dislocations are shown in green, blue, and pink; any other dislocation is shown in red.

occupied by atoms at the interface relative to the bulk, while IT represents the thickness of the space over which interfacial defects are concentrated. Values of the shear strength, right after JC and before the application of shear, are calculated and plotted as a function of these two parameters in Fig. 12. As an overall trend, it is seen that shear strength has a reverse relationship with IVE (Fig. 12(a)), and direct relationship with IT (Fig. 12(b)). The reverse relationship between shear strength and IVE heavily depends on the orientation of the interface plane. In other words, if only one color is used for all data points in Fig. 12(a), no clear trend could be seen on the graph. But the direct relationship between shear strength and IT is independent of the orientation of the interface plane (see Fig. 12(b)). This is an important observation as IT can potentially be used in a general way to predict shear strength.

The shear strength vs. IVE relationship can be explained by considering the fact that an increase in IVE is equivalent to having extra free volume near the interface, which in turn results in the contacting layers being farther away from each other. The larger the average distance between the contacting layers are, the loser the bond is. Therefore, it is easier for the contacting layers to move relative to each other leading to a lower value of shear strength. IT represents the thickness of the space near interface that dislocations exist in it. Therefore, the higher the IT is, the more dislocations are out of the plane of interface. During deformation, these dislocations need to move. Therefore, the higher the IT, the more resistance to deformation, and as a result, the higher the shear strength.

The aforementioned findings suggest that the values of IVE and IT right before applying shear can be used to explain or predict the deformation behavior of the interfaces under shear loading. IVE, or in general the existence of free volume at the interface compared to bulk, has been mentioned in the literature [23, 28, 50] and shown to be useful in providing insight into atomic-scale processes associated with stress-induced deformation. But, to the best of our knowledge, IT has never been quantified and used as done in this work. Its value right before deformation is informative on how concentrated the defects are in the space near the interface plane.

Conclusions

With the use of MD simulations, two aluminum substrates are placed at varied interfacial distances from one another and allowed to bond together through JC at room temperature. Then, the effect of 1) orientation of the atomic planes parallel to the interface, 2) misorientation of substrates with respect to each other, and 3) the strain normal to the interface due to JC (because of the initial gap between substrates before JC) on shear deformation is studied. It is seen that irrespective of misorientation or JC strain, (111)-oriented interfaces exhibit resistance-free sliding under shear loading, whereas in (001)- and (110)-oriented systems, shear is accommodated by dislocation multiplication (DM) initiated from the interface. DM triggers movement of dislocations from the interface toward the bulk and causes a substantial increase in the dislocation density in the system, which both immensely affect the material properties.

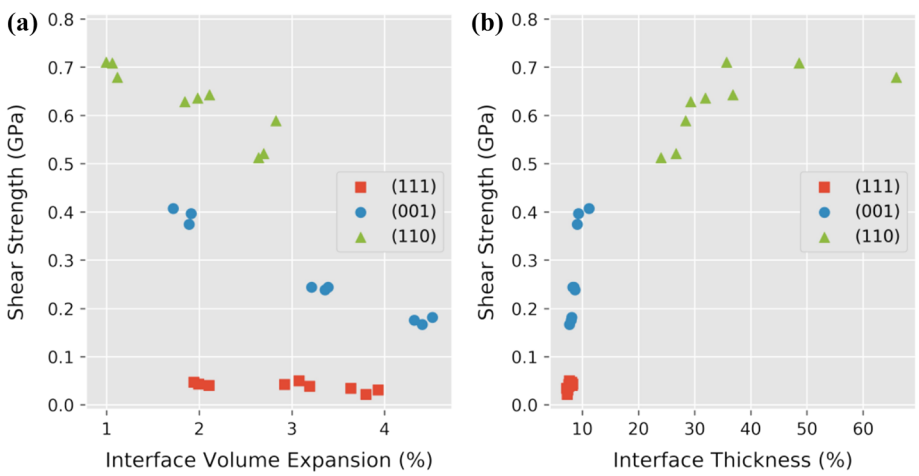

Figure 12 Shear strength of all the cases studied as a function of IVE (**a**) and IT (**b**) parameters calculated right before application of shear. Shear strength has a reverse relationship with IVE, for a specific orientation of the interface plane. Shear strength has a direct relationship with IT, independent of the orientation of the interface plane.

The change in the distribution of dislocations because of DM and their presence in the bulk can affect phase transformations and diffusional behavior of the material, i.e., altering the macroscopic material properties. The amount of DM that occurs for (001) and (110) systems increases by decrease in misorientation angle or increase in JC strain. Additionally, it is shown that the general characteristics of the profile of average atomic volume along the direction perpendicular to the interface can be used to explain the shear deformation behavior. Two parameters of interface volume expansion (IVE) (see Eq. 2) and interface thickness (IT) (see Eq. 3) are defined based on this profile. It is seen that IVE has a reverse and IT has a direct relationship with shear strength of the system. The reverse relationship between IVE and shear strength is found to be a function of the crystallographic orientation of the interface plane, whereas the direct relationship between IT and shear strength is shown to be independent of the interface plane. The IVE and IT parameters may be useful in connecting the results of atomistic simulations to macroscopic behavior of materials in numerous applications that involve shear deformation.

Acknowledgements

This work was supported by the National Science Foundation (CMMI-1728652) and the School of Engineering at Santa Clara University. Computing resources for running the LAMMPS simulations were provided by the Wiegand Advanced Visualization Environment (WAVE) at Santa Clara University.

Data availability

Data will be made available on request.

Declarations

Conflict of Interest The authors state that they have no known competing financial interests or personal relationships that could have appeared to influence the work presented in this article.

References

[1] Shah A, Gaul H, Schneider-Ramelow M, Reichl H, Mayer M, Zhou Y (2009) Ultrasonic friction power during Al wire wedge-wedge bonding. J Appl Phys 106:013503. https://doi.org/10.1063/1.3158065

[2] Seppänen H, Kurppa R, Meriläinen A, Hæggström E (2013) Real time contact resistance measurement to determine when microwelds start to form during ultrasonic wire bonding. Microelectron Eng 104:114–119. https://doi.org/10.1016/J.MEE.2012.12.003

[3] Kumar Rajak D, Pagar DD, Menezes PL, Eyvazian A (2020) Friction-based welding processes: friction welding and friction stir welding. J Adhes Sci Technol 34(24):2613–2637

[4] Heidarzadeh A, Mironov S, Kaibyshev R, Çam G, Simar A, Gerlich A, Khodabakhshi F, Mostafaei A, Field DP, Robson JD, Deschamps A, Withers PJ (2021) Friction stir welding/processing of metals and alloys: a comprehensive review on microstructural evolution. Prog Mater Sci 117:100752. https://doi.org/10.1016/J.PMATSCI.2020.100752

[5] Bakavos D, Prangnell PB (2010) Mechanisms of joint and microstructure formation in high power ultrasonic spot welding 6111 aluminium automotive sheet. Mater Sci Eng A 527:6320–6334. https://doi.org/10.1016/J.MSEA.2010.06.038

[6] Geissler U, Funck J, Schneider-Ramelow M, Engelmann HJ, Rooch I, Müller WH, Reichl H (2010) Interface formation in the US-Wedge/Wedge-bond process of AlSi1/CuNiAu contacts. J Electron Mater 40(2):239–246

[7] Smith J, Bozzolo G, Banerjea A, Ferrante J (1989) Avalanche in adhesion. Phys Rev Lett 63:1269–1272

[8] Mo Y, Turner KT, Szlufarska I (2009) Friction laws at the nanoscale. Nature 457(7233):1116–1119

[9] Luan B, Robbins MO (2005) The breakdown of continuum models for mechanical contacts. Nature 435(7044):929–932

[10] Gimzewski JK, Möller R (1987) Transition from the tunneling regime to point contact studied using scanning tunneling microscopy. Phys Rev B 36:1284–1287. https://doi.org/10.1103/PhysRevB.36.1284

[11] Agraït N, Rodrigo JG, Vieira S (1993) Conductance steps and quantization in atomic-size contacts. Phys Rev B 47:12345–12348. https://doi.org/10.1103/PhysRevB.47.12345

[12] Voets J, Keijsers RJP, Shklyarevskii OI, van Kempen H (1996) Effects of electrode interactions observed in a

mechanically controllable break junction. Phys Rev B 53:1072–1075. https://doi.org/10.1103/PhysRevB.53.1072

[13] Krans JM, Muller CJ, Yanson IK, Govaert TCM, Hesper R, van Ruitenbeek JM (1993) One-atom point contacts. Phys Rev B 48:14721–14724. https://doi.org/10.1103/PhysRevB.48.14721

[14] Landman U, Luedtke WD, Burnham NA, Colton RJ (1990) Atomistic mechanisms and dynamics of adhesion, nanoindentation, and fracture. Science 248:454–461. https://doi.org/10.1126/science.248.4954.454

[15] Khajehvand M, Sepehrband P (2018) The effect of crystallographic misorientation and interfacial separation on jump-to-contact behavior and defect generation in aluminum. Model Simul Mater Sci Eng 26(5):055007. https://doi.org/10.1088/1361-651X/aac427

[16] Khajehvand M, Seppänen H, Sepehrband P (2019) Nanoscale contact behavior of (1 1 1) fcc metallic surfaces. Comput Mater Sci 170:109149. https://doi.org/10.1016/j.commatsci.2019.109149

[17] Jiang H, Szlufarska I (2018) Small-angle twist grain boundaries as sinks for point defects. Sci Rep 8(1):1–3

[18] Shao S, Wang J, Misra A, Hoagland RG (2013) 2013 Spiral patterns of dislocations at nodes in (111) semi-coherent FCC interfaces. Sci. Reports 31(3):1–7. https://doi.org/10.1038/srep02448

[19] Guleryuz E, Mesarovic SD (2016) Dislocation nucleation on grain boundaries: low angle twist and asymmetric tilt boundaries. Crystals 6(7):77

[20] Wang J, Zhang RF, Zhou CZ, Beyerlein IJ, Misra A (2014) Interface dislocation patterns and dislocation nucleation in face-centered-cubic and body-centered-cubic bicrystal interfaces. Int J Plast 53:40–55. https://doi.org/10.1016/J.IJPLAS.2013.07.002

[21] Farkas D (2013) Atomistic simulations of metallic microstructures. Curr Opin Solid State Mater Sci 17:284–297. https://doi.org/10.1016/J.COSSMS.2013.11.002

[22] Bomarito GF, Lin Y, Warner DH (2015) An atomistic modeling survey of the shear strength of twist grain boundaries in aluminum. Scr Mater 101:72–75. https://doi.org/10.1016/J.SCRIPTAMAT.2015.01.022

[23] Tucker GJ, Tschopp MA, McDowell DL (2010) Evolution of structure and free volume in symmetric tilt grain boundaries during dislocation nucleation. Acta Mater 58:6464–6473. https://doi.org/10.1016/J.ACTAMAT.2010.08.008

[24] Tucker GJ, McDowell DL (2011) Non-equilibrium grain boundary structure and inelastic deformation using atomistic simulations. Int J Plast 27:841–857. https://doi.org/10.1016/J.IJPLAS.2010.09.011

[25] Sansoz F, Molinari JF (2005) Mechanical behavior of Σ tilt grain boundaries in nanoscale Cu and Al: A quasicontinuum study. Acta Mater 53:1931–1944. https://doi.org/10.1016/J.ACTAMAT.2005.01.007

[26] Lu Y, Huang JY, Wang C, Sun S, Lou J (2010) Cold welding of ultrathin gold nanowires. Nat Nanotechnol 5:218–224. https://doi.org/10.1038/nnano.2010.4

[27] Wan L, Wang S (2009) Shear response of the Σ11, ⟨1 1 0⟩ {1 3 1} symmetric tilt grain boundary studied by molecular dynamics. Model Simul Mater Sci Eng 17:045008. https://doi.org/10.1088/0965-0393/17/4/045008

[28] Yuasa M, Nakazawa T, Mabuchi M (2010) Atomic simulation of grain boundary sliding in Co/Cu two-phase bicrystals. Mater Sci Eng A 527:2629–2636. https://doi.org/10.1016/J.MSEA.2009.12.025

[29] Wang J, Misra A, Hirth JP (2011) Shear response of Σ 3 112 twin boundaries in face-centered-cubic metals. Phys Rev B 83(6):064106

[30] Raj R, Ashby MF (1971) On grain boundary sliding and diffusional creep. Metall Trans 4:1113–1127

[31] Van Swygenhoven H, Derlet PM (2001) Grain-boundary sliding in nanocrystalline fcc metals. Phys Rev B 64:224105. https://doi.org/10.1103/PhysRevB.64.224105

[32] Schönfelder B, Gottstein G, Shvindlerman LS (2005) Comparative study of grain-boundary migration and grain-boundary self-diffusion of [0 0 1] twist-grain boundaries in copper by atomistic simulations. Acta Mater 53:1597–1609. https://doi.org/10.1016/J.ACTAMAT.2004.12.010

[33] Daphalapurkar NP, Ramesh KT (2012) Orientation dependence of the nucleation and growth of partial dislocations and possible twinning mechanisms in aluminum. J Mech Phys Solids 60:277–294. https://doi.org/10.1016/J.JMPS.2011.10.009

[34] Plimpton S (1995) Fast Parallel Algorithms for Short-Range Molecular Dynamics. J Comput Phys 117:1–19. https://doi.org/10.1006/JCPH.1995.1039

[35] Sheng HW, Kramer MJ, Cadien A, Fujita T, Chen MW (2011) Highly optimized embedded-atom-method potentials for fourteen fcc metals. Phys Rev B 83:134118. https://doi.org/10.1103/PhysRevB.83.134118

[36] Nosé S (1984) A molecular dynamics method for simulations in the canonical ensemble. Mol Phys 52:255–268. https://doi.org/10.1080/00268978400101201

[37] Hoover WG (1985) Canonical dynamics: Equilibrium phase-space distributions. Phys Rev A 31:1695–1697. https://doi.org/10.1103/PhysRevA.31.1695

[38] Hoover WG (1986) Constant-pressure equations of motion. Phys Rev A 34:2499–2500. https://doi.org/10.1103/PhysRevA.34.2499

[39] Stukowski A, Bulatov VV, Arsenlis A (2012) Automated identification and indexing of dislocations in crystal interfaces. Model Simul Mater Sci Eng 20:085007. https://doi.org/10.1088/0965-0393/20/8/085007

[40] Stukowski A (2010) Visualization and analysis of atomistic simulation data with OVITO–the Open Visualization Tool. Model Simul Mater Sci Eng 18:015012. https://doi.org/10.1088/0965-0393/18/1/015012

[41] Dodaran M, Wang J, Chen Y, Meng WJ, Shao S (2019) Energetic, structural and mechanical properties of terraced interfaces. Acta Mater 171:92–107. https://doi.org/10.1016/J.ACTAMAT.2019.04.016

[42] Ogata S, Li J, Yip S (2002) Ideal pure shear strength of aluminum and copper. Sci 298(5594):807–811

[43] Yang L, Lai C, Li S (2019) Atomistic simulations of energies for arbitrary grain boundaries. Part II: Statistical analysis of energies for tilt and twist grain boundaries. Comput Mater Sci 162:268–276. https://doi.org/10.1016/J.COMMATSCI.2019.03.010

[44] Yin Q, Wang Z, Mishra R, Xia Z (2017) Atomic simulations of twist grain boundary structures and deformation behaviors in aluminum. AIP Adv 7:015040. https://doi.org/10.1063/1.4975042

[45] Wolf D (1989) Correlation between energy and volume expansion for grain boundaries in FCC metals. Scr Metall 23:1913–1918. https://doi.org/10.1016/0036-9748(89)90482-1

[46] Olmsted DL, Foiles SM, Holm EA (2009) Survey of computed grain boundary properties in face-centered cubic metals: I. Grain Bound Energy Acta Mater 57:3694–3703. https://doi.org/10.1016/J.ACTAMAT.2009.04.007

[47] Poletaev GM, Zorya IV, Starostenkov MD (2018) Role of point defects in self-diffusion along low-angle twist boundaries in fcc metals: a molecular dynamics study. J Micromech Mol Phys 3:1850001

[48] Poletaev GM, Martynov AN, Starostenkov MD (2010) The structure and energy of twist grain boundaries in fcc metals. Fundam Probl Sovrem Materialoved Basic Probl Mater Sci 7(4):27–34

[49] Dai S, Xiang Y, Srolovitz DJ (2014) Atomistic, generalized Peierls-Nabarro and analytical models for (1 1 1) twist boundaries in Al, Cu and Ni for all twist angles. Acta Mater 69:162–174. https://doi.org/10.1016/J.ACTAMAT.2014.01.022

[50] Spearot DE (2008) Evolution of the E structural unit during uniaxial and constrained tensile deformation. Mech Res Commun 35:81–88. https://doi.org/10.1016/J.MECHRESCOM.2007.09.002